Cell Reports, Volume *41*

Supplemental information

Mechanisms of IRF2BPL-related disorders and identification of a potential therapeutic strategy

Shrestha Sinha Ray, Debdeep Dutta, Cassandra Dennys, Samantha Powers, Florence Roussel, Pawel Lisowski, Petar Glažar, Xiaojin Zhang, Pipasha Biswas, Joseph R. Caporale, Nikolaus Rajewsky, Marc Bickle, Nicolas Wein, Hugo J. Bellen, Shibi Likhite, Paul C. Marcogliese, and Kathrin C. Meyer

Table S1: Cell lines used in the study.

Cell line	Age (yrs)	Mutation	Gender	Status	Disease severity
H1	8	N/A	Male	Healthy child	N/A
H2	8	N/A	Female	Healthy child	N/A
H3	65	N/A	Female	Healthy adult	N/A
H4	36	N/A	Male	Healthy adult	N/A
P1	12	p.E172X and p.G195V	Male	Child patient	Severe developmental regression[S1]
P2	10	p.Y173X	Male	Child patient	Severe developmental regression[S2]
P3	21	p.R188X	Male	Adult patient	Severe developmental regression[S1,2]
P4	3	p.A708Fs59	Male	Child patient	Mild developmental delay[S2]

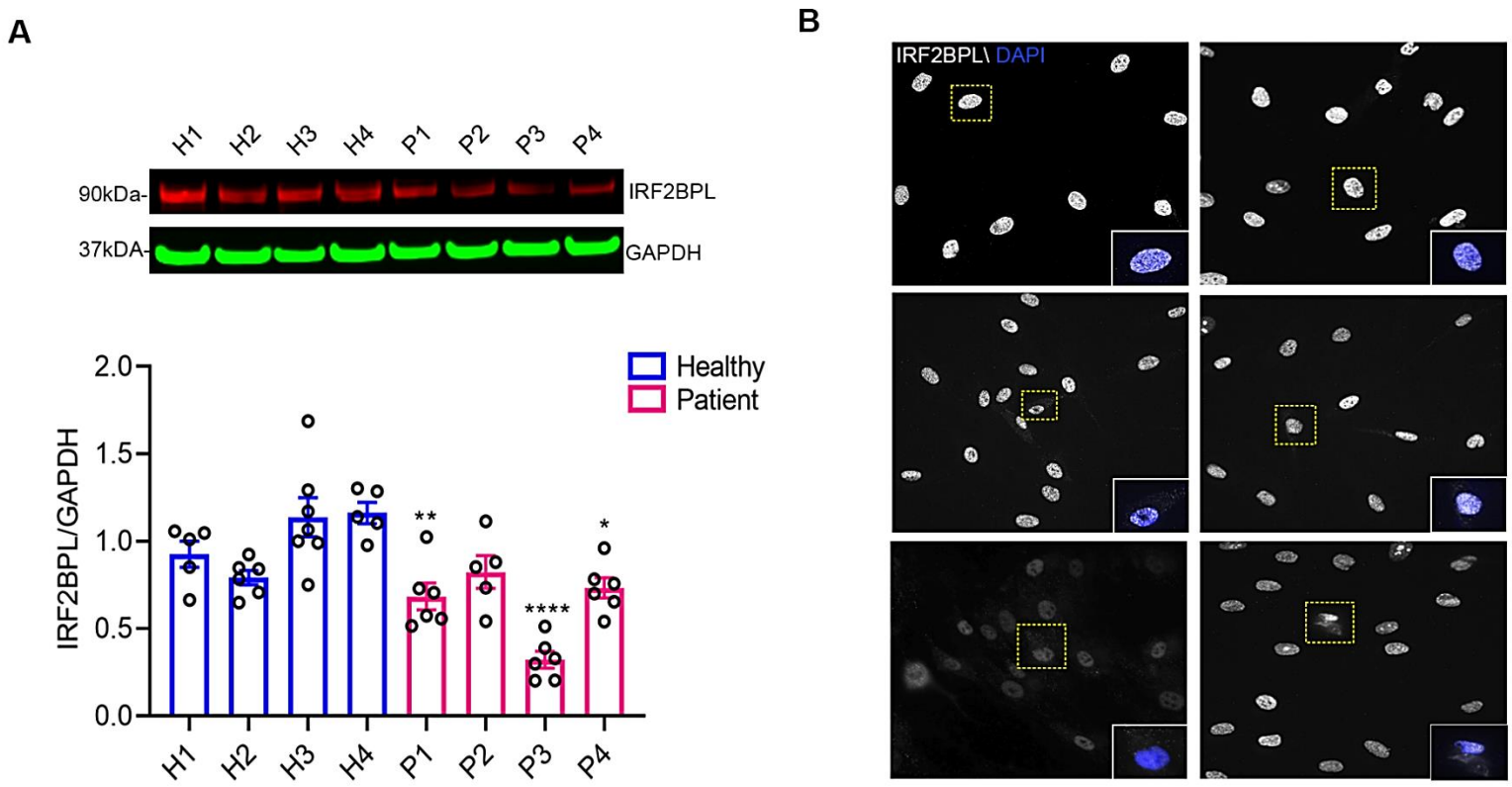

Figure S1: Comparison of IRF2BPL protein expression between NEDAMSS and healthy fibroblasts (A) and (B) show IRF2BPL expression levels of healthy and NEDAMSS fibroblasts by western blot and immunocytochemistry respectively. Only adult patient P3, shows approximately 50% lower expression compared to healthy lines. IRF2BPL protein smears are faintly seen in the cytoplasm of patient fibroblasts. Yellow dotted rectangles represent the merged image of DAPI and IRF2BPL stained cells seen in the corner white boxes (dimensions of image 40 µm x 50 µm) of each fibroblast cell line. ANOVA followed by Dunnett's multiple comparison test between the mean of the controls and the mean of each line was computed to derive the P value (p), * = $p < 0.05$, ** = $p < 0.01$, *** = $p < 0.001$, **** = $p < 0.0001$. Scale bar = 50µm.

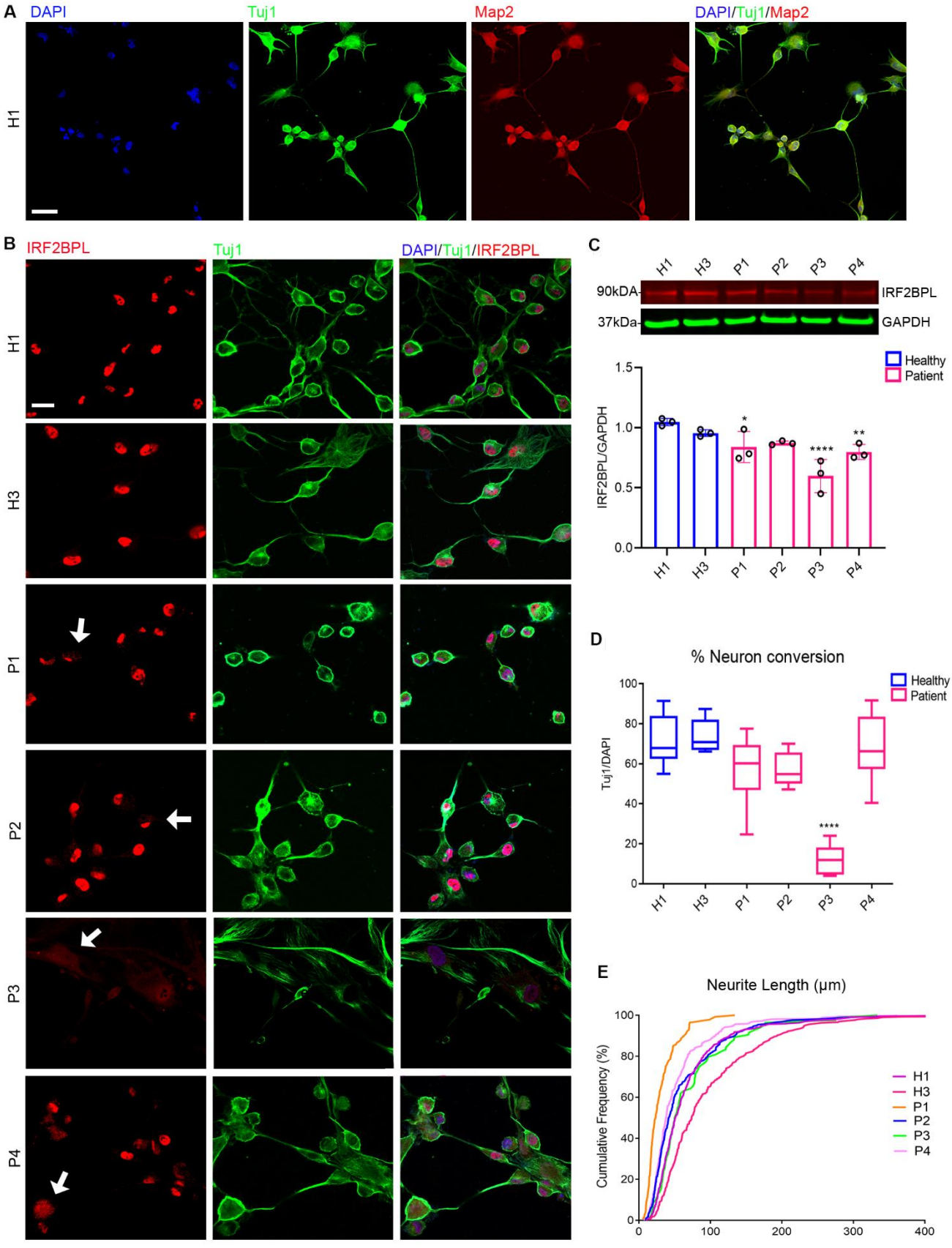
A
DAPI
Tuj1
Map2
DAPI/Tuj1/Map2
H1
B
IRF2BPL
Tuj1
DAPI/Tuj1/IRF2BPL
H1
H3
P1
P2
P3
P4
C
H1
H3
P1
P2
P3
P4
90kDA-
IRF2BPL
37kDa-
GAPDH
Healthy
Patient
IRF2BPL/GAPDH
1.5
1.0
0.5
0.0
*
****
**
D
% Neuron conversion
Healthy
Patient
Tuj1/DAPI
100
80
60
40
20
0
****
E
Neurite Length (μm)
Cumulative Frequency (%)
100
80
60
40
20
0
0
100
200
300
400
H1
H3
P1
P2
P3
P4

Figure S2: NEDAMSS patient neurons exhibit variable phenotype. Fibroblasts were directly converted to neurons (iNs) using seven small molecules: VPA, CHIR99021, repsox, forskolin, SP600125, GO6983 and Y-27632 (A) Flourescent microscope imaging at 40X magnification shows directly converted iNs from H1 fibroblasts express neuron specific markers Tuj1 and MAP2 on day 7. (B) Confocal two-dimensional imaging (63X/1.4 Oil magnification) shows IRF2BPL protein present as faint smears in the cytoplasm of Tuj1+ day 7 patient iNs in comparison to healthy iNs. White arrows indicate the protein smears. A representative image was selected for each line from three independent culture replicates (C) Western blot of IRF2BPL expression levels in healthy and patient iNs reveals the most significant loss of protein in line P3. Protein lysates from three replicates were tested (D) Neuronal conversion rate (% Tuj1 positive cells over total DAPI stained cells) and their (E) neurite length on day 7 indicates a range of phenotypes among NEDAMSS patient iNs, with patient P3 exhibiting significantly lower conversion rate and patients P1 and P3 displaying shorter neurite length. A total of 15 fields captured at 20X magnification from three differentiation experiments was analyzed by using ImageJ software. ANOVA followed by Dunnett's multiple comparison test between the mean of the controls and the mean of each line was computed to derive the P value (p), * = $p < 0.05$, ** = $p < 0.01$, *** = $p < 0.001$, **** = $p < 0.0001$. Scale bar for (a) 50µm and for (b) 20µm.

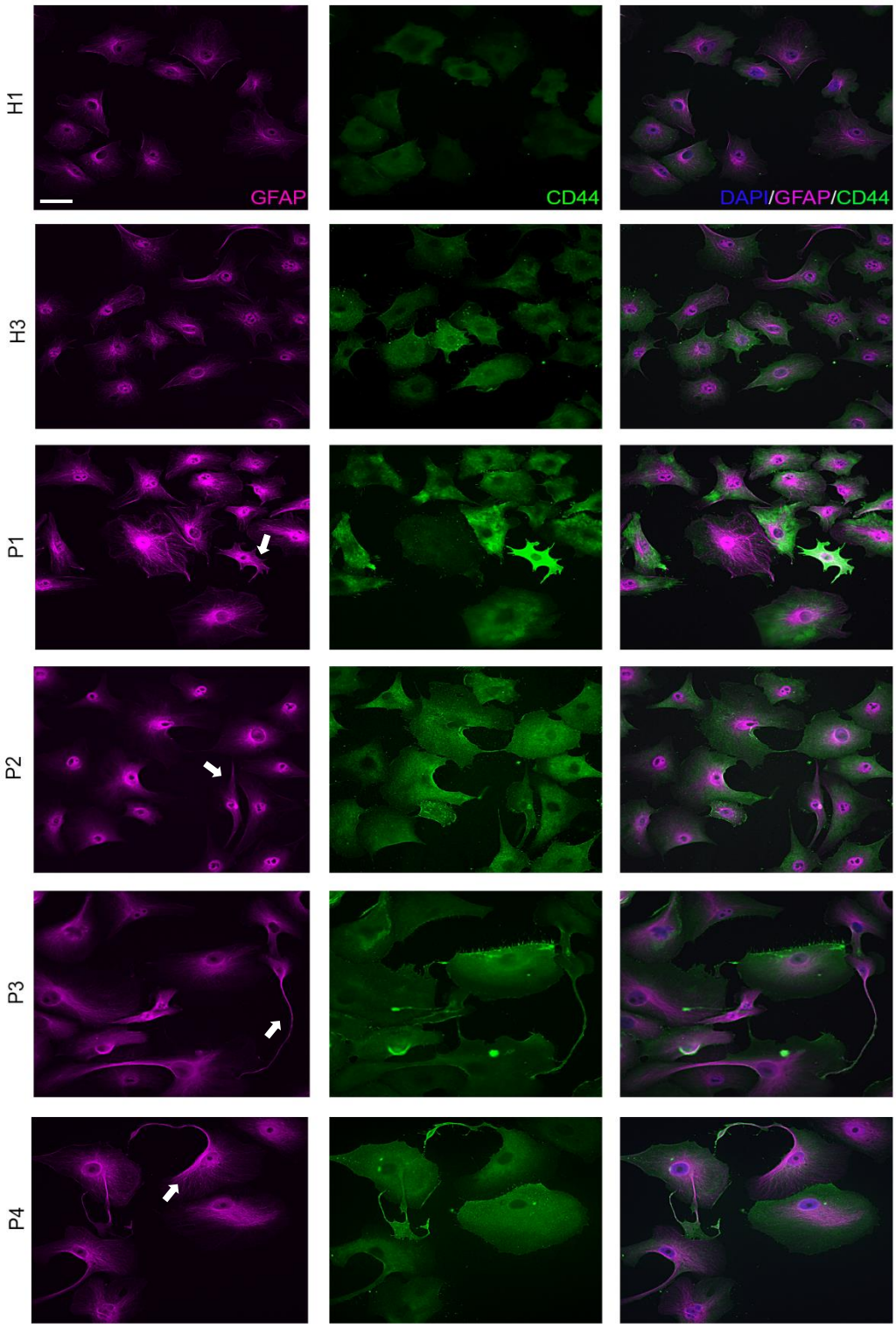

Figure S3: Characterization of differentiated astrocytes (iAs) from healthy and patient iNPCs. Healthy and NEDAMSS patient iAs are positive for astrocyte-specific markers GFAP and CD44. Patient iAs exhibit an activated phenotype compared to healthy iAs. Images from three independent experiments were captured at 40X magnification with Nikon Eclipse Ti2-E microscope. White arrows indicate morphological differences in NEDAMSS patient iAs compared to healthy cell lines. Scale bar = 50µm.

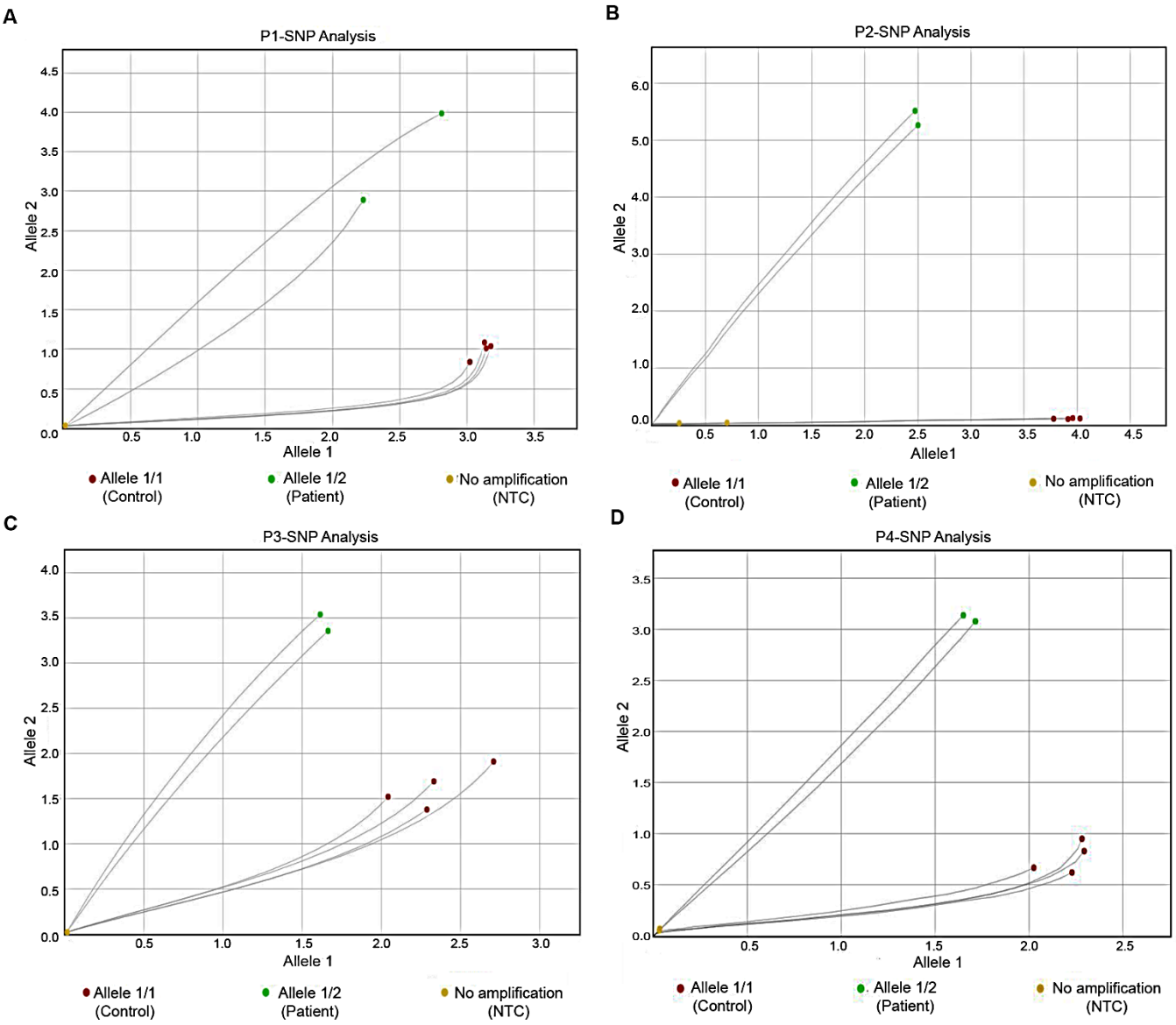

Figure S4: SNP genotyping analysis to detect the presence of mutant mRNA in patients. RNA from differentiated iAs from healthy lines (H1 and H3) and NEDAMSS patients (P1, P2, P3 and P4) was extracted and transcribed to cDNA. Customized SNP genotyping assay was conducted to detect the presence of the mutated and wildtype IRF2BPL mRNA in (A) P1 (c.514G>T and c.584G>T) (B) P2 (c.519C>G) (C) P3 (c.562C>T) and (D) P4 (c.2122delG) compared to healthy controls. Two different cell passages from each patient and control were used for the SNP analysis. The assay was repeated three times.

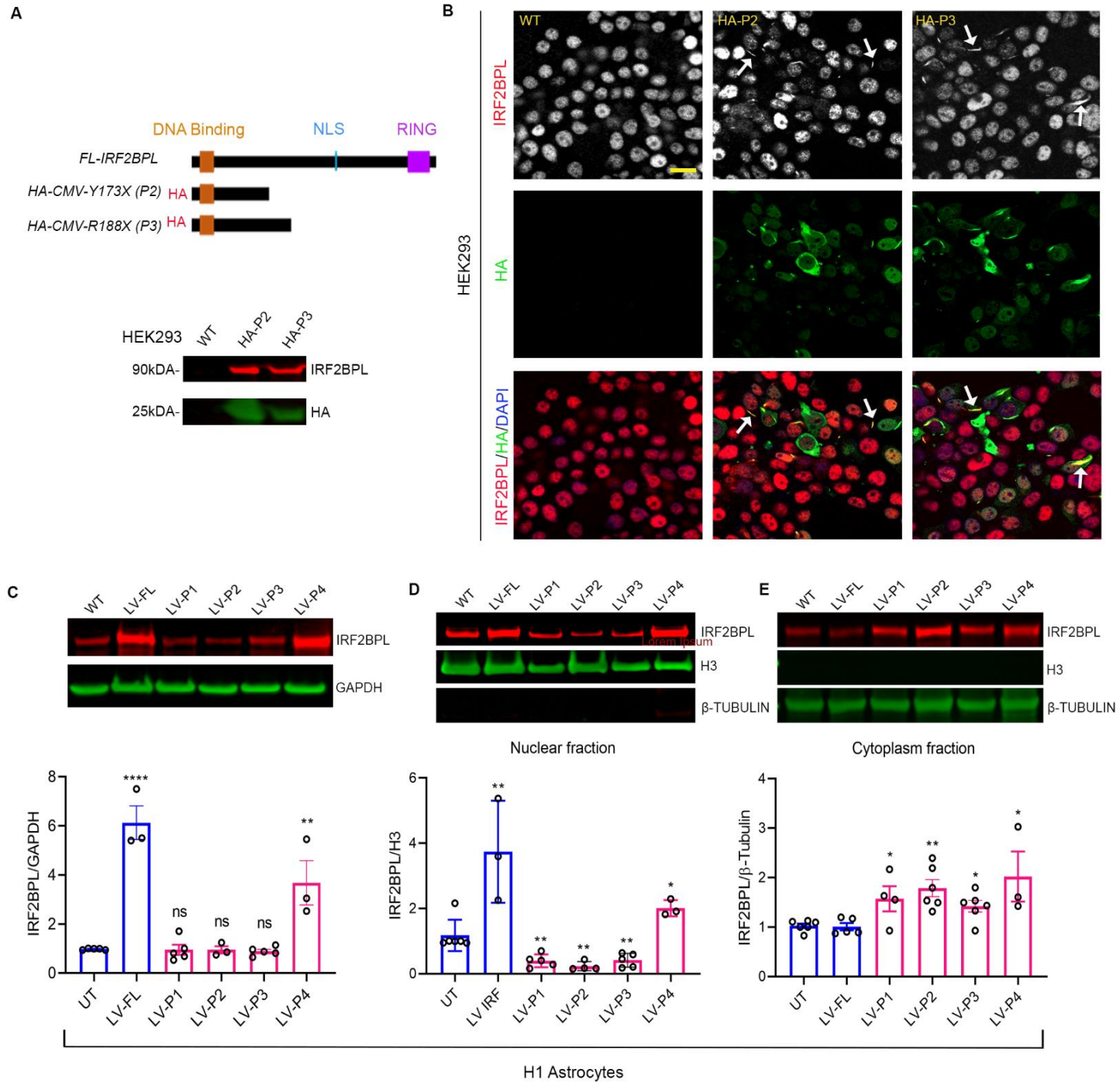

Figure S5: Overexpression of mutant IRF2BPL protein dimerizes with full length (FL) IRF2BPL and causes sequestration of the protein to the cytoplasm in HEK293s and in wildtype astrocyte line H1. (A) Schematic of constructs expressing N-terminal HA-tagged truncated IRF2BPL proteins (*HA-CMV-P2* and *HA-CMV-P3*). These constructs were transfected into HEK293s and pelleted down for HA pull down assay after 72 hours. HA elute blot confirms that FL-IRF2BPL (white, anti-IRF2BPL) and HA-tagged truncated IRF2BPL P2 or P3 (green, anti-HA) can bind to each other, as seen in lanes 2 and 3. (B) Confocal imaging indicates mis-localization of FL-IRF2BPL to the cytoplasm of HEK293 cells transfected with the constructs. White arrows point to FL-IRF2BPL protein mislocalized to the cytoplasm. Two-dimensional images were captured at 63X/1.4 Oil magnification covering 9 random fields from three independent replicates. (C) Healthy H1 iAs was transduced with lenti-virus (LV) expressing FL-IRF2BPL or the patient-derived truncated proteins for 4 days and pelleted down for western blot. LV-FL and LV-P4 showed higher levels of total IRF2BPL protein

expression compared to un-transduced (UT) astrocytes. Fractionation studies conducted on the same pellets revealed lower levels of IRF2BPL in the (D) nuclear fraction (normalized to nuclear marker H3) for iAs transduced with LV-P1, LV-P2 and LV-P3 and higher levels in the (E) cytoplasm fraction (normalized to cytoplasmic marker β-Tubulin), which further confirms sequestration of the full length to the cytoplasm by mutant proteins. All experiments were conducted with a minimum of three independent culture repeats. Unpaired t-test was conducted between un-transduced (UT) and each LV condition to derive the P value (p), * = $p < 0.05$, ** = $p < 0.01$, *** = $p < 0.001$, **** = $p < 0.0001$, ns = not significant. Scale bar = 50µm.

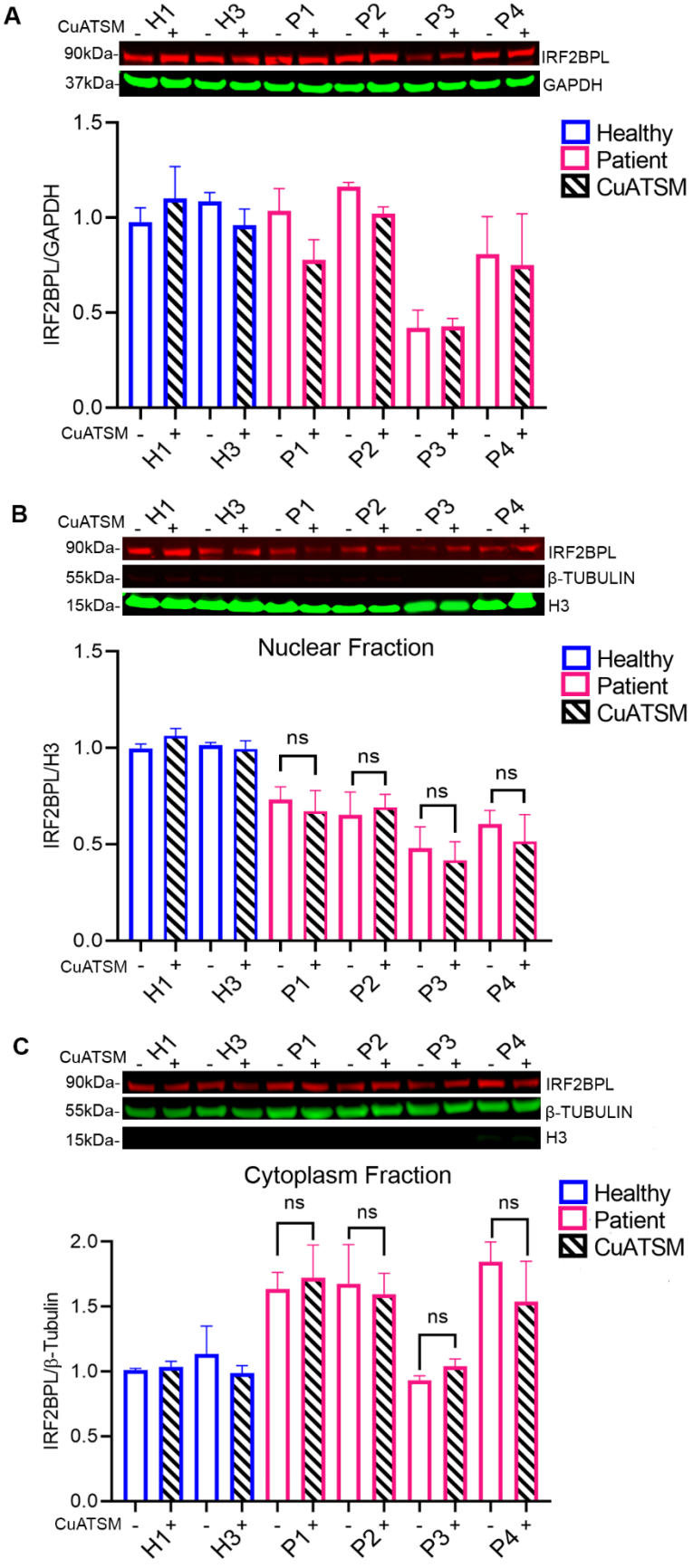
A
CuATSM - + - + - + - + - + - +
H1 H3 P1 P2 P3 P4
90kDa-
IRF2BPL
37kDa-
GAPDH
IRF2BPL/GAPDH
1.5
1.0
0.5
0.0
Healthy
Patient
CuATSM
B
55kDa-
β-TUBULIN
15kDa-
H3
Nuclear Fraction
IRF2BPL/H3
ns
C
Cytoplasm Fraction
IRF2BPL/β-Tubulin
2.0

Figure S6: CuATSM does not impact IRF2BPL expression levels or sequestration of the protein in patients. (A) Treatment with CuATSM does not change the overall expression of IRF2BPL in heathy and patient iAs. (B) Nuclear and (C) cytoplasmic fractions do not show any difference with drug treatment. Three independent culture replicates were used for the western blot. Unpaired t-test was conducted between untreated and treated groups to compute p value. ns= not significant.

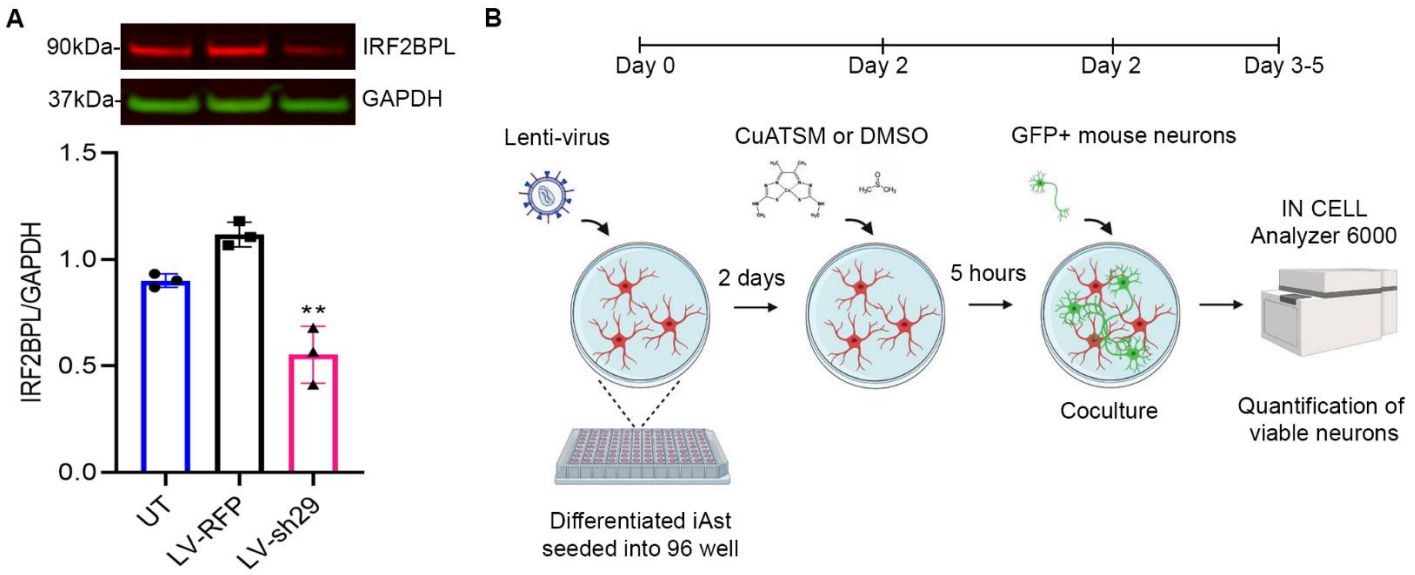

Figure S7: Knockdown of IRF2BPL protein by lentivirus expressing shRNA in H1 iAs. (A) H1 iAs was transduced with LV-RFP and LV-sh29 (expressing RFP and shRNA against IRF2BPL respectively) at an MOI of 10 and pelleted down after 4 days to assess the knockdown of protein by western blot. Experiment was repeated three times. Unpaired t-test was conducted between un-transduced (UT) iAs and LV-sh29 transduced iAs to compute P value (p). ** $p<0.01$. (B) Schematic of coculture assay depicts seeding of lentivirus (LV) transduced iAs with GFP+ mouse neurons. On day 2, CuATSM (1 µM) or DMSO was added to iAs, 5 hours before coculture with neurons. Illustration was created by using biorender.com.

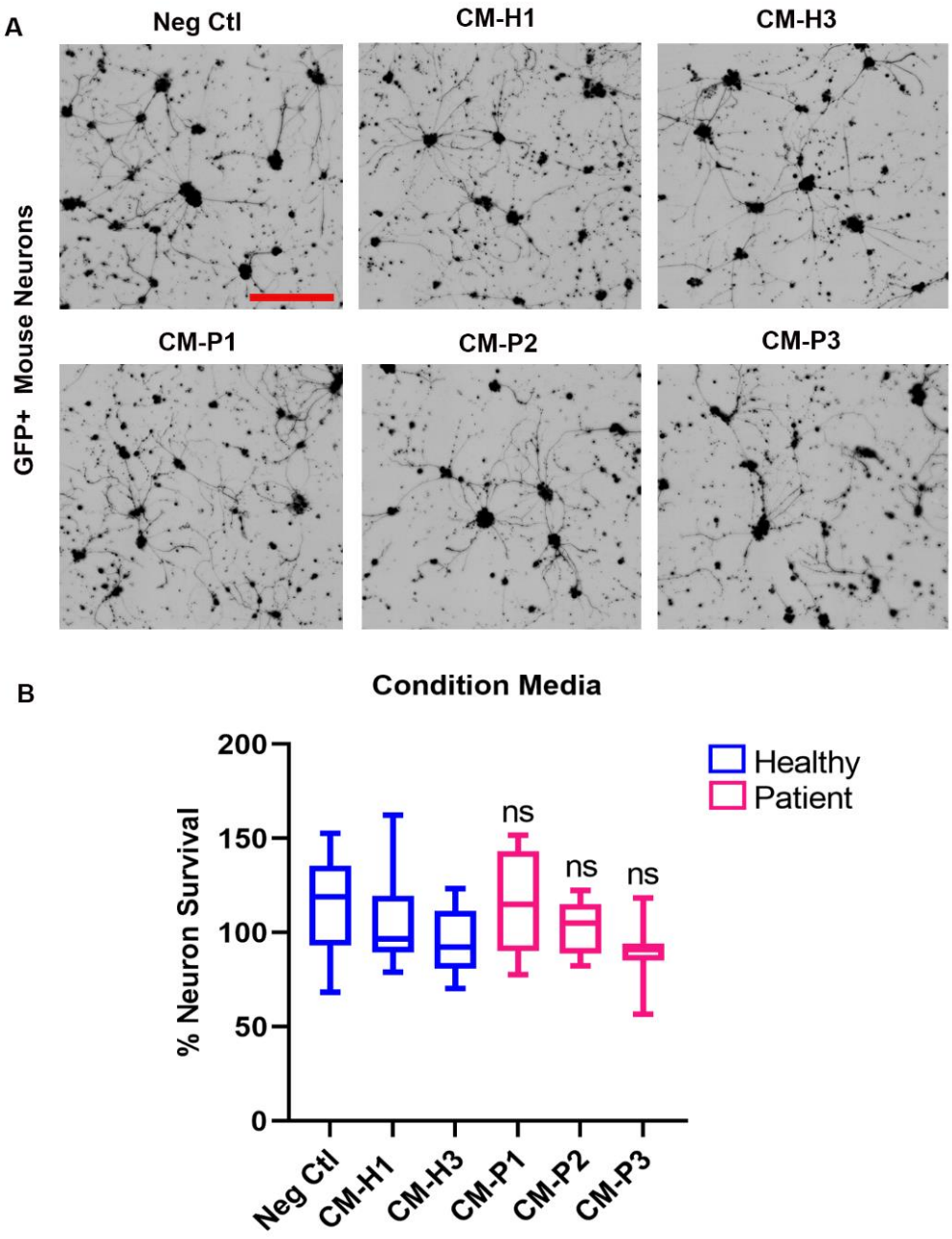

Figure S8: Condition media of NEDAMSS iAs has no effect on neuron viability. Control and patient iAs were seeded in triplicates in a 96 well plate (day 0) and the following day (day 1) the astrocyte media was replaced with neuron media. On day 1, GFP+ mouse neurons were seeded in triplicates in poly-lysine and laminin coated 96 well plate with fresh neuron media. For the next two days (day 2 and day 3), media of the neurons was replaced with 60% condition neuron media (CM) from each iAs cell line. Neg Ctl wells were replaced with fresh neuron media instead of CM. (A) Representative images of GFP+ mouse neurons (shown in black) following 48 hours in CM (day 4). (B) Quantification of neuronal survival on day 4 shows no significant loss of neuronal survival with patient iAs condition media compared to controls. Data was normalized to average neuronal survival of healthy controls and represents 3 independent culture repeats. ANOVA followed by Dunnett's multiple comparison test between the mean of the controls and the mean of each line was computed to derive the P value (p), ns= not significant. Scale bar= 200µm.

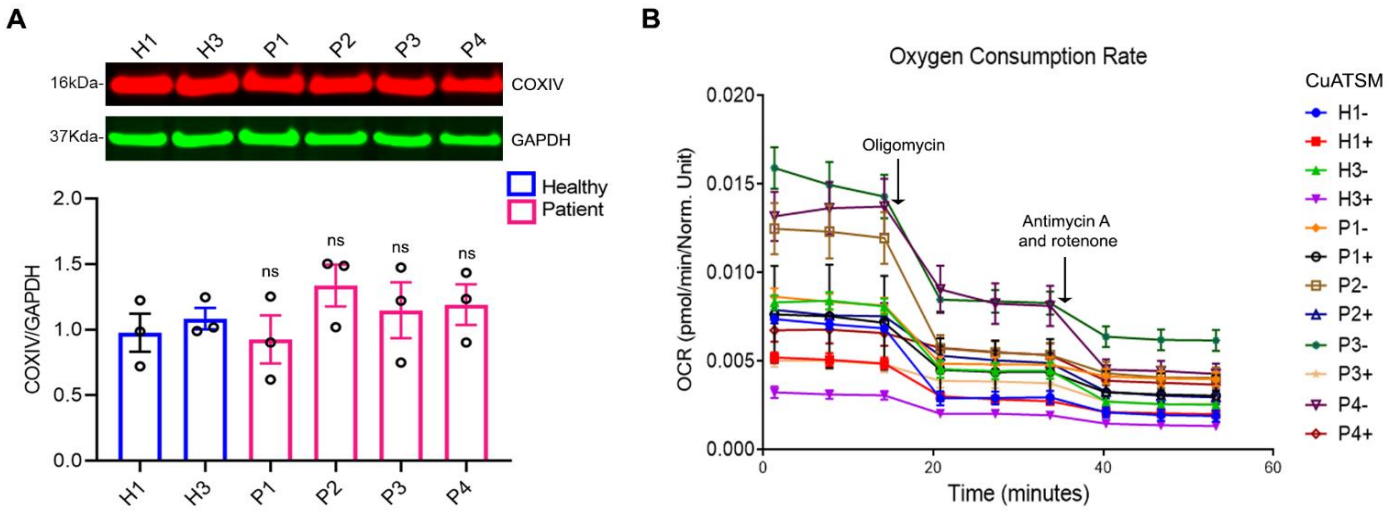

Figure S9: Mitochondrial COXIV expression remains intact in NEDAMSS iAs but the oxygen consumption rate shows elevated levels. (A) Differentiated iAs from healthy controls and patients were pelleted down after 5 days to quantify the expression levels of COXIV, a mitochondrial marker. ANOVA followed by Dunnett's multiple comparison test between the mean of the controls and the mean of each line was computed to derive the P value (p), ns= not significant, (B) Oxygen consumption rate (OCR) of iAs computed from Seahorse ATP rate assay with and without treatment with CuATSM. Experiment was repeated with three independent culture replicates.

Table S3: Thirty-seven common differentially expressed genes in patient iAs. [Reference]

	Log 2 FC	P Adjusted	Neuronal Function, Growth, Development, Support, Neurological Diseases	Mitochondria, Metabolism, Oxidation, Apoptosis
REG3G	-8.3000	0.03787		[S3,4]
LINC01593	-5.2000	0.01323		
SSTR2	-4.2600	0.01394	[S5-7]	[S7-9]
ABCA8	-3.8000	0.00893	[S10,11]	
ANKS1B	-3.6400	0.00563	[S12-18]	
LINC00639	-3.5900	0.00978		
CADPS	-3.1400	0.00008	[S19-22]	
EGR2	-3.1400	0.01323	[S23-28]	[S28,29]
UGT1A7	-3.0300	0.00281	[S30]	
LMOD1	-2.7100	0.00363		
AC138305.1	-2.2100	0.00746		
FAM71F1	-2.0700	0.02580		
KLF2	-1.6100	0.02705	[S31-33]	[S34-36]
STK32C	-1.2900	0.02462	[S37-39]	
SEMA4G	-1.0400	0.00056	[S40-43]	
MOCS1	-1.0100	0.01414	[S44-47]	[S48,49]
GRIP2	-0.6800	0.04881	[S50-52]	
NUDT18	-0.6300	0.04849		
ADGRF5	6.4800	0.00746		
GREB1L	5.2900	0.02536	[S53,54]	
ADGRV1	4.7600	0.00019	[S55-58]	
CDSN	4.6800	0.03052		
NLRP2	4.6100	0.02821	[S59,60]	
NRG2	4.4300	0.03979	[S61-64]	
GLDC	4.2600	0.00746	[S65,66]	
CPPED1	3.0400	0.00069		
PHACTR1	2.8500	0.02536	[S67-69]	
C6orf141	2.7700	0.00007		
ZNF469	2.3700	0.03713		
TNFAIP8	2.2900	0.02705		[S70-72]
DMKN	1.7300	0.03052		
EPB41L4B	1.5200	0.03713		
AKT3	1.4700	0.03713	[S73-76]	[S77,78]
]PLCXD2	1.4600	0.03052		
BTBD3	1.1100	0.04881	[S79,80]	
UBASH3B	1.0300	0.04013		
CYP4V2	0.9300	0.04881		

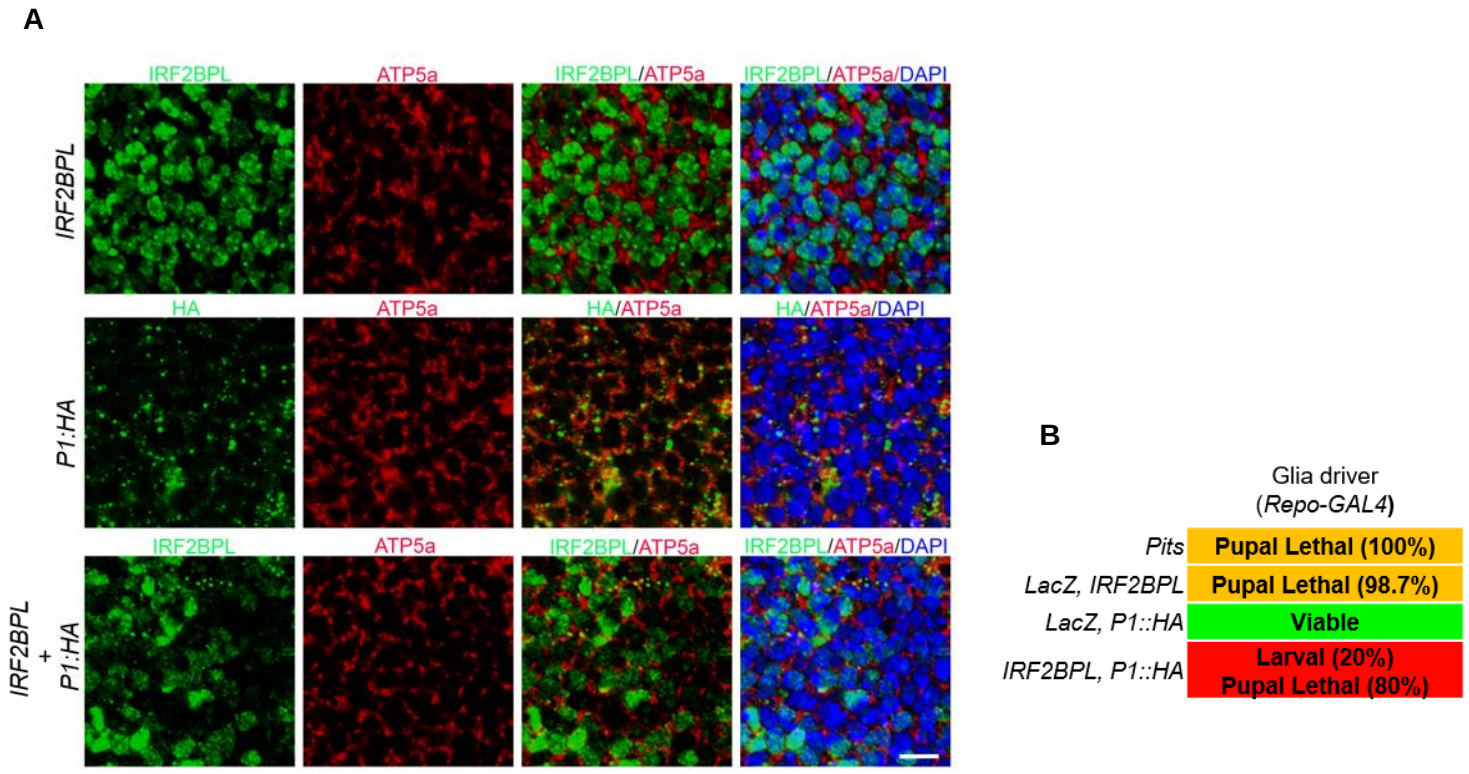

Figure S10: Overexpression of human IRF2BPL and patient-related truncation in *Drosophila* causes mislocalization of full-length IRF2BPL and causes pupal lethality. (A) Overexpression of *UAS-IRF2BPL* alone by nubbin-GAL4 driver, is primarily localized to nucleus in the wing pouch of *Drosophila* (anti-IRF2BPL in green), whereas *UAS-IRF2BPLp.E172X::HA* (*P1::HA*) alone is found mislocalized to the cytoplasm (anti-HA in green). When both the constructs are co-expressed, the full-length IRF2BPL is seen mislocalized to the cytoplasm (anti-IRF2BPL in green). ATP5a in red is a mitochondrial marker used. Scale bar = 2µm. (B) Overexpression of UAS-IRF2BPL in glia using Repo-GAL4 at 29°C causes pupal lethality. Overexpression of *UAS-IRF2BPLp.E172X::HA* alone leads to viable adults, however co-expression of full-length *UAS-IRF2BPL* and truncated *UAS-IRF2BPLp.E172X::HA* lead to larval and pupal lethality. These data indicate that there may be a toxic effect when both full-length and truncated proteins are expressed.

Table S5: List of primers used for mutagenesis

Construct	Forward primer (5'-3')	Reverse primer (5'-3')
pCDNA-HA-P1	GCCACCATGTACCCATACG	CTAGAAGCGGCTGCGCTGTTCCA
pCDNA-HA-P2	GCCACCATGTACCCATACG	CTACTCGAAGCGGCTGCGCTGTT
pCDNA-HA-P3	GCCACCATGTACCCATACG	TCACGCGGTGTGGCTGCTGCTT
UAS-P1::HA	GACCCAGCTTTCTTGTACAAAGTTG	GAAGCGGCTGCGCTGTTC

Table S6: List of primers used for quantitative PCR in the study

Gene	Forward primer (5'-3')	Reverse primer (5'-3')
SSTR2	CTGTGTACCAAGCCCCAGAT	GATGATCACCATGGCTGTGT
ERG2	GTGACCATCTTTCCCAATGC	TTGCCCATGTAAGTGAAGGTC
AKT3	CGGAAAGATTGTGTACCGTGATC	CTTCATGGTGGCTGCATCTGTG
NGR2	CAGAAGAGGGTCCTGACCATCA	GAGGTGGTTGTGCATCTGCTTC

References

S1. Marcogliese, P.C., Shashi, V., Spillmann, R.C., Stong, N., Rosenfeld, J.A., Koenig, M.K., Martinez-Agosto, J.A., Herzog, M., Chen, A.H., Dickson, P.I., et al. (2018). IRF2BPL Is Associated with Neurological Phenotypes. Am J Hum Genet *103*, 245-260. 10.1016/j.ajhg.2018.07.006.

S2. Tran Mau-Them, F., Guibaud, L., Duplomb, L., Keren, B., Lindstrom, K., Marey, I., Mochel, F., van den Boogaard, M.J., Oegema, R., Nava, C., et al. (2019). De novo truncating variants in the intronless IRF2BPL are responsible for developmental epileptic encephalopathy. Genet Med *21*, 1008-1014. 10.1038/s41436-018-0143-0.

S3. Chen, Z., Downing, S., and Tzanakakis, E.S. (2019). Four Decades After the Discovery of Regenerating Islet-Derived (Reg) Proteins: Current Understanding and Challenges. Front Cell Dev Biol *7*. 10.3389/FCELL.2019.00235.

S4. Xiang, M., Li, S., Zhou, H., Xie, M., Zhang, Z., Gou, J., Yang, J., Tian, C., Ma, K., Lu, Y., et al. (2021). Reg3g ameliorates Tacrolimus-induced pancreatic β cell dysfunction by restoring mitochondrial function. Authorea. 10.22541/AU.161695374.47072563/V1.

S5. Bowman, B.R., Bokiniec, P., McMullan, S., Goodchild, A.K., and Burke, P.G.R. (2019). Somatostatin 2 Receptors in the Spinal Cord Tonically Restrain Thermogenic, Cardiac and Other Sympathetic Outflows. Front Neurosci *0*, 121. 10.3389/FNINS.2019.00121.

S6. Kumar, U. (2005). Expression of somatostatin receptor subtypes (SSTR1–5) in Alzheimer's disease brain: An immunohistochemical analysis. Neuroscience *134*, 525-538. 10.1016/J.NEUROSCIENCE.2005.04.001.

S7. Stumm, R.K., Zhou, C., Schulz, S., Endres, M., Kronenberg, G., Allen, J.P., Tulipano, G., and Hollt, V. (2004). Somatostatin receptor 2 is activated in cortical neurons and contributes to neurodegeneration after focal ischemia. J Neurosci *24*, 11404-11415. 10.1523/JNEUROSCI.3834-04.2004.

S8. Lehman, J., Hoeksema, M., Qian, J., Chen, H., Shi, C., Eisenberg, R., and Massion, P.P. (2016). Loss of somatostatin receptor 2 expression and cellular metabolism and survival in small cell lung cancer. ASCO *34*, e20090-e20090. 10.1200/JCO.2016.34.15_SUPPL.E20090.

S9. Maduro, V., Pusey, B.N., Cherukuri, P.F., Atkins, P., Du Souich, C., Rupps, R., Limbos, M., Adams, D.R., Bhatt, S.S., Eydoux, P., et al. (2016). Complex translocation disrupting TCF4 and altering TCF4 isoform expression segregates as mild autosomal dominant intellectual disability. Orphanet J Rare Dis *11*. 10.1186/s13023-016-0439-6.

S10. Bleasel, J.M., Hsiao, J.-H.T., Halliday, G.M., and Kim, W.S. (2013). Increased Expression of ABCA8 in Multiple System Atrophy Brain is Associated with Changes in Pathogenic Proteins. J Parkinson's Dis *3*, 331-339. 10.3233/JPD-130203.

S11. Kim, Woojin S., Hsiao, J.-Hsiang T., Bhatia, S., Glaros, Elias N., Don, Anthony S., Tsuruoka, S., Shannon Weickert, C., and Halliday, Glenda M. (2013). ABCA8 stimulates sphingomyelin production in oligodendrocytes. Biochem J *452*, 401-410. 10.1042/BJ20121764.

S12. Carbonell, A.U., Cho, C.H., Tindi, J.O., Counts, P.A., Bates, J.C., Erdjument-Bromage, H., Cvejic, S., Iaboni, A., Kvint, I., Rosensaft, J., et al. (2019). Haploinsufficiency in the ANKS1B gene encoding AIDA-1 leads to a neurodevelopmental syndrome. Nat Commun*10*, 1-15.

S13. Dosemeci, A., Toy, D., Reese, T.S., and Tao-Cheng, J.-H. (2015). AIDA-1 Moves out of the Postsynaptic Density Core under Excitatory Conditions. PLOS ONE *10*, e0137216. 10.1371/JOURNAL.PONE.0137216.

S14. Ghersi, E., Vito, P., Lopez, P., Abdallah, M., and D'Adamio, L. (2004). The intracellular localization of amyloid beta protein precursor (AbetaPP) intracellular domain associated protein-1 (AIDA-1) is regulated by AbetaPP and alternative splicing. J Alzeimer's Dis *6*, 67-78. 10.3233/JAD-2004-6108.

S15. Jacob, A.L., Jordan, B.A., and Weinberg, R.J. (2010). The organization of amyloid-β protein precursor intracellular domain-associated protein-1 in the rat forebrain. J Comp Neurol *518*, 3221. 10.1002/CNE.22394.
S16. Jordan, B.A., Fernholz, B.D., Khatri, L., and Ziff, E.B. (2007). Activity-dependent AIDA-1 nuclear signaling regulates nucleolar numbers and protein synthesis in neurons. Nat Neurosci *10*, 427-435. 10.1038/nn1867.
S17. Shi, M., Huang, X.-Y., Ren, X.-Y., Wei, X.-Y., Ma, Y., Lin, Z.-Z., Liu, D.-T., Song, L., Zhao, T.-J., Li, G., et al. (2021). AIDA directly connects sympathetic innervation to adaptive thermogenesis by UCP1. Nat Cell Biol *23*, 268-277. 10.1038/s41556-021-00642-9.
S18. Tindi, J., Chávez, A., Cvejic, S., Calvo-Ochoa, E., Castillo, P., and Jordan, B. (2015). ANKS1B Gene Product AIDA-1 Controls Hippocampal Synaptic Transmission by Regulating GluN2B Subunit Localization. J Neurosci *35*, 8986-8996. 10.1523/JNEUROSCI.4029-14.2015.
S19. Ishii, C., Shibano, N., Yamazaki, M., Arima, T., Kato, Y., Ishii, Y., Shinoda, Y., Fukazawa, Y., Sadakata, T., Sano, Y., and Furuichi, T. (2021). CAPS1 is involved in hippocampal synaptic plasticity and hippocampus-associated learning. Sci Rep *11*, 1-15. 10.1038/s41598-021-88009-w.
S20. Sadakata, T., Kakegawa, W., Shinoda, Y., Hosono, M., Katoh-Semba, R., Sekine, Y., Sato, Y., Tanaka, M., Iwasato, T., Itohara, S., et al. (2013). CAPS1 Deficiency Perturbs Dense-Core Vesicle Trafficking and Golgi Structure and Reduces Presynaptic Release Probability in the Mouse Brain. J Neurosci *33*, 17326-17334. 10.1523/JNEUROSCI.2777-13.2013.
S21. Shinoda, Y., Ishii, C., Fukazawa, Y., Sadakata, T., Ishii, Y., Sano, Y., Iwasato, T., Itohara, S., and Furuichi, T. (2016). CAPS1 stabilizes the state of readily releasable synaptic vesicles to fusion competence at CA3–CA1 synapses in adult hippocampus. Sci Rep *6*, 1-8. 10.1038/srep31540.
S22. Shumate, K.M., Tas, S.T., Kavalali, E.T., Emeson, R.B., KM, S., ST, T., ET, K., RB, E., Shumate, K.M., Tas, S.T., et al. (2021). RNA editing-mediated regulation of calcium-dependent activator protein for secretion (CAPS1) localization and its impact on synaptic transmission. J Neurochem *158*, 182-196. 10.1111/JNC.15372.
S23. Blanco-Canto, M.E., Patel, N., Velasco-Aviles, S., Casillas-Bajo, A., Salas-Felipe, J., Garcia-Escriva, A., Diaz-Marin, C., and Cabedo, H. (2020). Novel EGR2 variant that associates with Charcot-Marie-Tooth disease when combined with lipopolysaccharide-induced TNF-alpha factor T49M polymorphism. Neurol Genet *6*, e407. 10.1212/NXG.0000000000000407.
S24. Boerkoel, C.F., Takashima, H., Bacino, C.A., Daentl, D., and Lupski, J.R. (2001). EGR2 mutation R359W causes a spectrum of Dejerine-Sottas neuropathy. Neurogenetics *3*, 153-157. 10.1007/S100480100107.
S25. Kim, S.H., Song, J.Y., Joo, E.J., Lee, K.Y., Shin, S.Y., Lee, Y.H., Ahn, Y.M., and Kim, Y.S. (2011). Genetic association of the EGR2 gene with bipolar disorder in Korea. Exp Mol Med *44*, 121-129. 10.3858/emm.2012.44.2.007.
S26. Mukherjee, D., Gonzales, B.J., Ashwal-Fluss, R., Turm, H., Groysman, M., and Citri, A. (2021). Egr2 induction in SPNs of the ventrolateral striatum contributes to cocaine place preference in mice. eLife *10*. 10.7554/ELIFE.65228.
S27. Nagarajan, R., Svaren, J., Le, N., Araki, T., Watson, M., and Milbrandt, J. (2001). EGR2 Mutations in Inherited Neuropathies Dominant-Negatively Inhibit Myelin Gene Expression. Neuron *30*, 355-368. 10.1016/S0896-6273(01)00282-3.
S28. Zhang, P., Chen, Y., Zhang, S., Fang, M., Lin, X., Liu, T., Zhou, Y., Yu, X., and Chen, G. (2020). Egr2 upregulation induced mitochondrial iron overload implicating in sevoflurane-induced cognitive deficits in developing mice. Preprint from Research Square. 10.21203/RS.3.RS-131690/V1.
S29. Unoki, M., and Nakamura, Y. (2003). EGR2 induces apoptosis in various cancer cell lines by direct transactivation of BNIP3L and BAK. Oncogene *22*, 2172-2185. 10.1038/sj.onc.1206222.

S30. Gradinaru, D., Minn, A.L., Artur, Y., Minn, A., and Heydel, J.M. (2012). Effect of oxidative stress on UDP-glucuronosyltransferases in rat astrocytes. Toxicol Lett *213*, 316-324. 10.1016/J.TOXLET.2012.07.014.

S31. Enenstein, J., Milbauer, L., Domingo, E., Wells, A., Roney, M., Kiley, J., Wei, P., and Hebbel, R. (2010). Proinflammatory phenotype with imbalance of KLF2 and RelA: risk of childhood stroke with sickle cell anemia. Am J Hematol *85*, 18-23. 10.1002/AJH.21558.

S32. Shi, H., Sheng, B., Zhang, F., Wu, C., Zhang, R., Zhu, J., Xu, K., Kuang, Y., Jameson, S., Lin, Z., et al. (2013). Kruppel-like factor 2 protects against ischemic stroke by regulating endothelial blood brain barrier function. Am J Physiol - Heart Circ *304*. 10.1152/AJPHEART.00712.2012.

S33. Wu, C., Li, F., Han, G., and Liu, Z. (2013). Aβ(1-42) disrupts the expression and function of KLF2 in Alzheimer's disease mediated by p53. Biochem Biophys Res Commun *431*, 141-145. 10.1016/J.BBRC.2013.01.008.

S34. Doddaballapur, A., Michalik, K.M., Manavski, Y., Lucas, T., Houtkooper, R.H., You, X., Chen, W., Zeiher, A.M., Potente, M., Dimmeler, S., and Boon, R.A. (2015). Laminar Shear Stress Inhibits Endothelial Cell Metabolism via KLF2-Mediated Repression of PFKFB3. Arterioscler Thromb Vasc Biol *35*, 137-145. 10.1161/ATVBAHA.114.304277.

S35. Maity, J., Deb, M., Greene, C., and Das, H. (2020). KLF2 regulates dental pulp-derived stem cell differentiation through the induction of mitophagy and altering mitochondrial metabolism. Red Biol *36*, 101622. 10.1016/J.REDOX.2020.101622.

S36. Yambire, K.F., Fernandez-Mosquera, L., Steinfeld, R., Mühle, C., Ikonen, E., Milosevic, I., and Raimundo, N. (2019). Mitochondrial biogenesis is transcriptionally repressed in lysosomal lipid storage diseases. eLife *8*. 10.7554/ELIFE.39598.

S37. Dempster, E., Wong, C., Lester, K., Burrage, J., Gregory, A., Mill, J., and Eley, M. (2014). Genome-wide methylomic analysis of monozygotic twins discordant for adolescent depression. Biol Psychiatry *76*, 977-983. 10.1016/J.BIOPSYCH.2014.04.013.

S38. Gasparoni, G., Bultmann, S., Lutsik, P., Kraus, T.F.J., Sordon, S., Vlcek, J., Dietinger, V., Steinmaurer, M., Haider, M., Mulholland, C.B., et al. (2018). DNA methylation analysis on purified neurons and glia dissects age and Alzheimer's disease-specific changes in the human cortex. Epigenetics Chromatin 2018 11:1 *11*, 1-19. 10.1186/S13072-018-0211-3.

S39. Starnawska, A., Hansen, C.S., Sparsø, T., Mazin, W., Olsen, L., Bertalan, M., Buil, A., Bybjerg-Grauholm, J., Bækvad-Hansen, M., Hougaard, D.M., et al. (2017). Differential DNA methylation at birth associated with mental disorder in individuals with 22q11.2 deletion syndrome. Transl Psychiatry *7*, e1221-e1221. 10.1038/tp.2017.181.

S40. Gurrapu, S., and Tamagnone, L. (2016). Transmembrane semaphorins: Multimodal signaling cues in development and cancer. Cell Adh Migr *10*, 675. 10.1080/19336918.2016.1197479.

S41. Li, H., Wu, D., and Sullivan, S. (1999). Characterization and expression of sema4g, a novel member of the semaphorin gene family. Mech Dev *87*, 169-173. 10.1016/S0925-4773(99)00125-2.

S42. Maier, V., Jolicoeur, C., H, R., Takegahara, N., Kumanogoh, A., Kikutani, H., Tessier-Lavigne, M., Wurst, W., and Friedel, R. (2011). Semaphorin 4C and 4G are ligands of Plexin-B2 required in cerebellar development. Mol Cell Neurosci *46*, 419-431. 10.1016/J.MCN.2010.11.005.

S43. Tseveleki, V., Rubio, R., Vamvakas, S.-S., White, J., Taoufik, E., Petit, E., Quackenbush, J., and Probert, L. (2010). Comparative gene expression analysis in mouse models for multiple sclerosis, Alzheimer's disease and stroke for identifying commonly regulated and disease-specific gene changes. Genomics *96*, 82. 10.1016/J.YGENO.2010.04.004.

SS44. Arenas, M., Fairbanks, L.D., Vijayakumar, K., Carr, L., Escuredo, E., and Marinaki, A.M. (2009). An unusual genetic variant in the MOCS1 gene leads to complete missplicing of an alternatively spliced exon in a patient with molybdenum cofactor deficiency. J Inherit Metab Dis *32*, 560-569. 10.1007/S10545-009-1151-7.

S45. Lee, H.-J., Adham, I.M., Schwarz, G., Kneussel, M., Sass, J.O., Engel, W., and Reiss, J. (2002). Molybdenum cofactor-deficient mice resemble the phenotype of human patients. Hum Mol Genet *11*, 3309-3317. 10.1093/HMG/11.26.3309.

S46. Mayr, S., Sass, J., Vry, J., Kirschner, J., Mader, I., Hövener, J., Reiss, J., Santamaria-Araujo, J., Schwarz, G., and Grünert, S. (2018). A mild case of molybdenum cofactor deficiency defines an alternative route of MOCS1 protein maturation. J Inherit Metab Dis *41*, 187-196. 10.1007/S10545-018-0138-7.

S47. Reiss, J., Christensen, E., Kurlemann, G., Zabot, M., and Dorche, C. (1998). Genomic structure and mutational spectrum of the bicistronic MOCS1 gene defective in molybdenum cofactor deficiency type A. Hum Genet *103*, 639-644. 10.1007/S004390050884.

S48. Grings, M., Seminotti, B., Karunanidhi, A., Ghaloul-Gonzalez, L., Mohsen, A.-W., Wipf, P., Palmfeldt, J., Vockley, J., and Leipnitz, G. (2019). ETHE1 and MOCS1 deficiencies: Disruption of mitochondrial bioenergetics, dynamics, redox homeostasis and endoplasmic reticulum-mitochondria crosstalk in patient fibroblasts. Sci Rep *9*, 1-13. 10.1038/s41598-019-49014-2.

S49. Mayr, S.J., Röper, J., and Schwarz, G. (2020). Alternative splicing of the bicistronic gene molybdenum cofactor synthesis 1 (MOCS1) uncovers a novel mitochondrial protein maturation mechanism. J Biol Chem *295*, 3029-3039. 10.1074/JBC.RA119.010720.

S50. Dong, H., Zhang, P., Song, I., Petralia, R., Liao, D., and Huganir, R. (1999). Characterization of the glutamate receptor-interacting proteins GRIP1 and GRIP2. J Neurosci *19*, 6930-6941. 10.1523/JNEUROSCI.19-16-06930.1999.

S51. Mao, L., Takamiya, K., Thomas, G., Lin, D.-T., and Huganir, R.L. (2010). GRIP1 and 2 regulate activity-dependent AMPA receptor recycling via exocyst complex interactions. Proc Nat Acad Sci U S A *107*, 19038-19043. 10.1073/PNAS.1013494107.

S52. Takamiya, K., Mao, L., Huganir, R.L., and Linden, D.J. (2008). The glutamate receptor-interacting protein family of GluR2-binding proteins is required for long-term synaptic depression expression in cerebellar Purkinje cells. J Neurosci *28*, 5752-5755. 10.1523/JNEUROSCI.0654-08.2008.

S53. Schrauwen, I., Liaqat, K., Schatteman, I., Bharadwaj, T., Nasir, A., Acharya, A., Ahmad, W., Van Camp, G., and Leal, S. (2020). Autosomal Dominantly Inherited GREB1L Variants in Individuals with Profound Sensorineural Hearing Impairment. Genes *11*, 1-18. 10.3390/GENES11060687.

S54. Schrauwen, I., Kari, E., Mattox, J., Llaci, L., Smeeton, J., Naymik, M., Raible, D.W., Knowles, J.A., Crump, J.G., Huentelman, M.J., and Friedman, R.A. (2018). De Novo variants in GREB1L are associated with non-syndromic inner ear malformations and deafness. Hum Genet *137*, 459. 10.1007/S00439-018-1898-8.

S55. Lau, S.-F., Cao, H., Fu, A.K.Y., and Ip, N.Y. (2020). Single-nucleus transcriptome analysis reveals dysregulation of angiogenic endothelial cells and neuroprotective glia in Alzheimer's disease. Proc Nat Acad Sci U S A *117*, 25800-25809. 10.1073/PNAS.2008762117.

S56. Liu, Z., Ye, X., Zhang, J., Wu, B., Dong, S., and Gao, P. (2021). Biallelic ADGRV1 variants are associated with Rolandic epilepsy. Neurol Sci 10.1007/S10072-021-05403-Y.

S57. Myers, K., Nasioulas, S., Boys, A., McMahon, J., Slater, H., Lockhart, P., Sart, D., and Scheffer, I. (2018). ADGRV1 is implicated in myoclonic epilepsy. Epilepsia *59*, 381-388. 10.1111/EPI.13980.

S58. Yan, W., Long, P., Chen, T., Liu, W., Yao, L., Ren, Z., Li, X., Wang, J., Xue, J., Tao, Y., et al. (2018). A Natural Occurring Mouse Model with Adgrv1 Mutation of Usher Syndrome 2C and Characterization of its Recombinant Inbred Strains. Cell Physiol Biochem *47*, 1883-1897. 10.1159/000491068.

S59. Minkiewicz, J., de Rivero Vaccari, J., and Keane, R. (2013). Human astrocytes express a novel NLRP2 inflammasome. Glia *61*, 1113-1121. 10.1002/GLIA.22499.

S60. Vizlin-Hodzic, D., Zhai, Q., Illes, S., Södersten, K., Truvé, K., Parris, T., Sobhan, P., Salmela, S., Kosalai, S., Kanduri, C., et al. (2017). Early onset of inflammation during ontogeny of bipolar disorder: the NLRP2 inflammasome gene distinctly differentiates between patients and healthy controls in the transition between iPS cell and neural stem cell stages. Transl Psychiatry *7*. 10.1038/TP.2016.284.

S61. Lee, K., Lee, H., Yang, C., Ko, J., Park, C., RS, W., Kim, J., Sun, W., Kim, J., Ho, W., and Lee, S. (2015). Bidirectional Signaling of Neuregulin-2 Mediates Formation of GABAergic Synapses and Maturation of Glutamatergic Synapses in Newborn Granule Cells of Postnatal Hippocampus. J Neurosci *35*, 16479-16493. 10.1523/JNEUROSCI.1585-15.2015.
S62. Longart, M., Liu, Y., Karavanova, I., and Buonanno, A. (2004). Neuregulin-2 is developmentally regulated and targeted to dendrites of central neurons. J Comp Neurol *472*, 156-172. 10.1002/cne.20016.
S63. Nakano, N., Kanekiyo, K., Nakagawa, T., Asahi, M., and Ide, C. (2016). NTAK/neuregulin-2 secreted by astrocytes promotes survival and neurite outgrowth of neurons via ErbB3. Neuroscie Lett *622*, 88-94. 10.1016/J.NEULET.2016.04.050.
S64. Yan, L., Shamir, A., Skirzewski, M., Leiva-Salcedo, E., Kwon, O.B., Karavanova, I., Paredes, D., Malkesman, O., Bailey, K.R., Vullhorst, D., et al. (2017). Neuregulin-2 ablation results in dopamine dysregulation and severe behavioral phenotypes relevant to psychiatric disorders. Mol Psychiatry *23*, 1233-1243. 10.1038/mp.2017.22.
S65. Coughlin, C.R., Swanson, M.A., Kronquist, K., Acquaviva, C., Hutchin, T., Rodríguez-Pombo, P., Väisänen, M.-L., Spector, E., Creadon-Swindell, G., Brás-Goldberg, A.M., et al. (2016). The genetic basis of classic nonketotic hyperglycinemia due to mutations in GLDC and AMT. Genet Med *19*, 104-111. 10.1038/gim.2016.74.
S66. Pai, Y.J., Leung, K.-Y., Savery, D., Hutchin, T., Prunty, H., Heales, S., Brosnan, M.E., Brosnan, J.T., Copp, A.J., and Greene, N.D.E. (2015). Glycine decarboxylase deficiency causes neural tube defects and features of non-ketotic hyperglycinemia in mice. Nat Commun *6*. 10.1038/NCOMMS7388.
S67. Freilinger, T., Anttila, V., Vries, B.d., Malik, R., Kallela, M., Terwindt, G.M., Pozo-Rosich, P., Winsvold, B., Nyholt, D.R., Oosterhout, W.P.J.v., et al. (2012). Genome-wide association analysis identifies susceptibility loci for migraine without aura. Nat Genet *44*, 777. 10.1038/NG.2307.
S68. Hamada, N., Ogaya, S., Nakashima, M., Nishijo, T., Sugawara, Y., Iwamoto, I., Ito, H., Maki, Y., Shirai, K., Baba, S., et al. (2018). De novo PHACTR1 mutations in West syndrome and their pathophysiological effects. Brain *141*, 3098-3114. 10.1093/BRAIN/AWY246.
S69. Ito, H., Mizuno, M., Noguchi, K., Morishita, R., Iwamoto, I., Hara, A., and Nagata, K.i. (2018). Expression analyses of Phactr1 (phosphatase and actin regulator 1) during mouse brain development. Neurosci Res *128*, 50-57. 10.1016/J.NEURES.2017.08.002.
S70. Garcia, J., Ferreira, H., Vieira, F., Gameiro, R., Andrade, A., Eugênio, F., Flores, E., and Cardoso, T. (2017). Tumour necrosis factor-alpha-induced protein 8 (TNFAIP8) expression associated with cell survival and death in cancer cell lines infected with canine distemper virus. Vet Comp Oncol *15*, 336-344. 10.1111/VCO.12168.
S71. Li, T., Wang, W., Gong, S., Sun, H., Zhang, H., Yang, A.-G., Chen, Y.H., and Li, X. (2018). Genome-wide Analysis Reveals TNFAIP8L2 as an Immune Checkpoint Regulator of Inflammation and Metabolism. Mol Immunol *99*, 154-162. 10.1016/j.molimm.2018.05.007
S72. Niture, S., Lin, M., Odera, J.O., Moore, J., Zhe, H., Chen, X., Suy, S., Collins, S.P., and Kumar, D. (2021). TNFAIP8 drives metabolic reprogramming to promote prostate cancer cell proliferation. Int J Biochem Cell Biol *130*, 105885. 10.1016/J.BIOCEL.2020.105885.
S73. Alcantara, D., Timms, A., Gripp, K., Baker, L., Park, K., Collins, S., Cheng, C., Stewart, F., Mehta, S., Saggar, A., et al. (2017). Mutations of AKT3 are associated with a wide spectrum of developmental disorders including extreme megalencephaly. Brain *140*, 2610-2622. 10.1093/BRAIN/AWX203.
S74. Howell, K.R., Floyd, K., and Law, A.J. (2017). PKBγ/AKT3 loss-of-function causes learning and memory deficits and deregulation of AKT/mTORC2 signaling: Relevance for schizophrenia. PLOS ONE *12*, e0175993. 10.1371/JOURNAL.PONE.0175993.
S75. Lopes, F., Torres, F., Soares, G., van Karnebeek, C.D., Martins, C., Antunes, D., Silva, J., Muttucomaroe, L., Botelho, L.F., Sousa, S., et al. (2019). The Role of AKT3 Copy Number Changes in

Brain Abnormalities and Neurodevelopmental Disorders: Four New Cases and Literature Review. Front Genet *0*, 58. 10.3389/FGENE.2019.00058.

S76. Zhang, T., Ding, H., Wang, Y., Yuan, Z., Zhang, Y., Chen, G., Xu, Y., and Chen, L. (2021). Akt3-mTOR regulates hippocampal neurogenesis in adult mouse. J Neurochem. 10.1111/JNC.15441.

S77. Kim, M., Kim, Y.Y., Jee, H.J., Bae, S.S., Jeong, N.Y., Um, J.-H., and Yun, J. (2016). Akt3 knockdown induces mitochondrial dysfunction in human cancer cells. Acta Biochim Biophys Sin *48*, 447-453. 10.1093/ABBS/GMW014.

S78. Polytarchou, C., Hatziapostolou, M., Yau, T.O., Christodoulou, N., Hinds, P.W., Kottakis, F., Sanidas, I., and Tsichlis, P.N. (2020). Akt3 induces oxidative stress and DNA damage by activating the NADPH oxidase via phosphorylation of p47(phox). Proc Natl Acad Sci U S A *117*, 28806-28815. 10.1073/pnas.2017830117.

S79. Matsui, A., Tran, M., Yoshida C., A., Kikuchi, S.S., Mami, U., Ogawa, M., and Shimogori, T. (2013). BTBD3 controls dendrite orientation toward active axons in mammalian neocortex. Science *342*, 1114-1118. 10.1126/science.1244505

S80. Thompson, S., Welch, A., Ho, E., Bessa, J., Portugal-Nunes, C., Morais, M., Young, J., Knowles, J., and Dulawa, S. (2019). Btbd3 expression regulates compulsive-like and exploratory behaviors in mice. Transl Psychiatry *9*. 10.1038/S41398-019-0558-7.